PCCP

Accepted Manuscript

ROYAL SOCIETY OF CHEMISTRY

www.rsc.org/pccp

Molecular Dynamics Study of Interfacial Thermal Transport between Silicene and Substrate

Jingchao Zhang[1], Yang Hong[2], Zhen Tong[3], Zhihuai Xiao[4,*], Hua Bao[3], Yanan Yue[4,*]

[1]Holland Computing Center, University of Nebraska-Lincoln, Lincoln, NE 68588, USA

[2]Department of Chemistry, University of Nebraska-Lincoln, Lincoln, NE 68588, USA

[3]University of Michigan-Shanghai Jiao Tong University Joint Institute, Shanghai Jiao Tong University, Shanghai 200240, China

[4]School of Power and Mechanical Engineering, Wuhan University, Wuhan, Hubei 430072, China

In this work, the interfacial thermal transport across silicene and various substrates, *i.e.*, crystalline silicon (*c*-Si), amorphous silicon (*a*-Si), crystalline silica (*c*-SiO_2) and amorphous silica (*a*-SiO_2) are explored by classical molecular dynamics (MD) simulations. A transient pulsed heating technique is applied in this work to characterize the interfacial thermal resistance in all hybrid systems. It is reported that the interfacial thermal resistances between silicene and all substrates decrease nearly 40% with temperature from 100 K to 400 K, which is due to the enhanced phonon couplings from anharmonicity effect. The phonon power spectra analysis for all systems is performed to interpret simulation results. Contradictory to the traditional thought that amorphous structures intend to have poor thermal transport capabilities due to the disordered atomic configurations, it is calculated that amorphous silicon and silica substrates facilitate the interfacial thermal transport compared with their crystalline structures. Besides, the coupling effect from substrate can improve the interface thermal transport up to 43.5 % for coupling strengths χ from 1.0 to 2.0. Our results provide fundamental knowledge and rational guidelines

*Corresponding author: Zhihuai Xiao, E-mail: xiaozhihuai@126.com; and Yanan Yue, E-mail: yyue@whu.edu.cn

for the design and development of the next-generation silicene-based nanoelectronics and thermal interface materials.

Silicene, analogous to graphene, is a two-dimensional (2D) monolayer of silicon atoms constructed in hexagonal lattices with a slight local buckling.[1] It has attracted great attentions due to its exceptionally high crystallinity and unusual electronic properties.[2-4] In contrast with the high thermal conductivity (κ) of graphene, the in-plane thermal conductivity of silicene is reported around 20-60 W/m·K, which is much lower than that of crystalline silicon (~140 W/m·K at room temperature).[5-7] The high electric transport capability and low thermal conductivity of silicene makes it a promising thermoelectric material for next generation nano-devices and offers new insights for low-dimensional materials and related applications.

Phonon thermal transport in the lateral directions of silicene nanoribbon (SNR) has been investigated by various numerical studies. Using NEMD method, Zhou *et al*.[8] calculated the κ of SNR at 61.7 and 68.5 W/m·K respectively for armchair and zigzag boundaries. Yang *et al*.[9] predicted the phonon lattice conductivity of silicene around 26 W/m·K using first principle calculations, which is much lower than that of bulk silicon (~140 W/m·K) . Also using first-principles calculation with single mode relaxation time approximation, Xie *et al*.[10] predicted a lower thermal conductivity of silicene (around 10 W/m·K). A thermal conductivity value at 5.5 W/m·K is calculated using equilibrium molecular dynamics (EMD) approach for all sizes considered.[11] Due to the special buckling structure in silicene, it is reported that its in-plane thermal conductivity can be tuned by applying proper tensile strains to distort the hexagonal lattice structures.[7]

Despite the fact that in-plane phonon thermal transport in silicene has been studied extensively, the interfacial thermal transport across silicene and substrate materials remains intact. To address this issue, thermal transport across silicene and multiple substrates (*c*-Si, *a*-Si, *c*-SiO_2, *a*-SiO_2) are calculated in this work. A fast transient technique is applied to characterize the thermal contact resistance (*R*) in the hybrid structures. Effects of temperature, substrate crystallinity and interfacial coupling strength are discussed to comprehensively understanding the interface thermal transport across atomic silicene structure and substrate. Phonon power spectra analysis for the hybrid silicene substrate systems is performed to interpret the calculated results.

In recent studies of silicene, quite a few empirical potentials have been proposed to describe the Si-Si interactions in silicene. Tersoff potential[12] has been widely used to describe the Si atom interactions in bulk silicon and silicon nanotubes. Wang *et al*.[13], Li *et al*.[14] and Hu *et al*.[2] employed the Tersoff potential to investigate the thermal conductivity of free-standing and supported single layer silicene. The calculated bond length and thermal conductivities of silicene are in good agreement with the predictions from first principles.[15-17] While on the other hand, due to the Tersoff potential employed, the buckled structure of silicene was not captured and the system has a planar equilibrium structure. The modified Tersoff potential by Kumagai *et al*.[18] preserved the forms of Tersoff potential functions and soundly reproduced the elastic constants of diamond silicon as well as the cohesive energies and equilibrium bond lengths of silicon polytypes. The proposed angular-dependent term is critical to give an improved description of the melting point. In this work, this modified Tersoff potential is found to be able to maintain the buckled structure in free standing silicene with a buckling distance of 0.64 Å. Considering its inheritance from the Tersoff potential and the improved features, the authors employed it to

describe the Si-Si interactions in monolayer silicene. In other studies, Pei *et al*.[7] used the MEAM potential[19] to explore the dependence of thermal conductivity of silicene on tensile stain and isotopic doping. Liu *et al*.[20] calculated the thermal conductivity using both Tersoff and Stillinger–Weber (SW) potentials.[21] Using a modified SW potential, Zhang *et al*.[11] characterized the thermal conductivity of silicene using non-equilibrium molecular dynamics. Some discrepancies exist among the calculated thermal conductivities with different potentials, but the calculated results are all on the same magnitude.

MD calculations in the work are performed by using the large-scale atomic/molecular massively parallel simulator (LAMMPS).[22] The interactions between Si-Si, Si-O atoms in silicene and *c*-Si, *a*-Si, *c*-SiO_2 and *a*-SiO_2 substrates are described by the Tersoff potentials.[18,23] Couplings between silicene and substrates are modeled by Lennard-Jones (LJ) potential $V(\mathrm{r}) = 4\chi\varepsilon[(\sigma/\mathrm{r})^{12} - (\sigma/\mathrm{r})^{6}]$, where ε and σ are the energy and distance parameters with units eV and Å respectively; χ represents the coupling strength between substrate material and the supported silicene. The ε and σ values are calculated from the universal force field (UFF),[24] where $\varepsilon_{Si\text{-}Si}$ = 0.0174398 eV, $\sigma_{Si\text{-}Si}$ = 3.8264 Å, $\varepsilon_{Si\text{-}O}$ = 0.0067376 eV and $\sigma_{Si\text{-}O}$ = 3.4542 Å. Cutoff distance r_c equals $3.5\sigma_{Si\text{-}Si}$ for Si-Si interactions and $3.5\sigma_{Si\text{-}O}$ for Si-O interactions. Atomic configurations of the hybrid systems are shown in Figs. 1(a)-(d). Distance between silicene and substrates is set as 4.295 Å. An initial buckling distance of 0.85 Å is used in the silicene structures, which is proved to be the stable distance in previous MD study,[7] and within the range of 0.44 – 1 Å from *ab. initio* calculations.[15,25,26] Periodic boundary conditions are applied to the lateral (*x* and *y*) directions of both silicene and the substrates. Free boundary condition is used in

the out-of-plane (z) direction. To remain consistent, the same silicene with dimensions of 105.374 × 95.4 ($x \times y$) Å^2 are used in all hybrid structures. A slight lattice mismatch of 1.74% and 3.68% are induced to the c-Si and c-SiO_2 substrates to fit the lattice parameter of silicene. Dimensions of c-Si, a-Si, c-SiO_2 and a-SiO_2 equal 105.374 × 94.704 × 85.386 Å^3 ($x \times y \times z$), 105.374 × 95.4 × 89.997 Å^3 ($x \times y \times z$), 105.231 × 95.662 × 87.002 Å^3 ($x \times y \times z$) and 105.374 × 95.4 × 89.663 Å^3 ($x \times y \times z$) respectively. A time step of 0.5 fs (1 fs = 10^{-15} s) is used for all calculations.

NEMD simulations are widely used to calculate the thermal contact resistance (R) at the interfaces of bulk heterostructures. After the hybrid system reaches equilibrium state, two groups of atoms are selected to add/substrate thermal energies respectively. After a steady temperature gradient is established, the interfacial thermal resistance can be calculated by the equation

$$R = \frac{\Delta T \cdot A}{q}, \tag{1}$$

where ΔT is the temperature bias, A is the cross-section area, and q is the heat flux along the heat conduction direction. Using this approach, R between SiC and graphite is calculated at ~(1-7) × 10^{-10} K·m^2/W.[27] Subbarayan *et al*.[28] calculated R between Si and SiO_2 to be (0.503-0.518) × 10^{-9} K·m^2/W. For 2D materials like graphene and silicene, thermal resistance in the lateral direction can also be calculated by the NEMD method. Zhang *et al*.[29] characterized the Kapitza resistance in the bending areas of graphene at 1.48 × 10^{-11} K·m^2/W at temperature 300 K. Thermal contact resistance at graphene-silicene monolayer is calculated at ~4 × 10^{-9} K·m^2/W.[30] In traditional NEMD simulations, when a heat flux is constantly imposed on a group of atoms, the local

temperatures in the heating/cooling areas are altered by variations of the atomic velocities. The energy exchange in/near the heated areas is very fast and kinetic and potential energies are unbalanced. Therefore, the temperatures recorded near the heat baths could be illusory. In hybrid bulk systems, the heat baths are normally distant from the hetero interfaces. After the temperature gradient reaches steady state in NEMD calculations, the temperature bias (ΔT) across the interface will be recorded and used to calculate the thermal resistance. Temperature points adjacent to the interfaces from both sides are used to characterize the temperature difference. This is a popular approach for R calculations which has been successfully applied in various systems.[31-35] While for membrane systems like silicene, the NEMD method for R characterization might not be applicable since the heat baths will be directly applied to the monolayer atomic structure. For this reason, the transient pulse heating approach is applied in this work.

Similar method has been applied to calculate interfacial thermal resistance at various 2D interfaces such as silicene/graphene,[36] boron-nitride/graphene,[37] MoS_2/graphene,[38] graphene/silicon[39] and graphene/copper.[40] For example, in the silicene/*c*-Si hybrid system, after 300 ps (1 ps = 10^{-12} s) canonical ensemble (*NVT*) calculations, the system reaches steady state at 300 K. Consecutively, another 200 ps microcanonical ensemble (*NVE*) calculations are performed to allow the system to be fully relaxed. Then a 50 fs (1 fs = 10^{-15} s) ultrafast thermal impulse is applied to the supported silicene, as is shown in Fig. 1(a). After the heat impulse, temperature of the silicene ($T_{silicene}$) reaches ~650 K while temperature of *c*-Si ($T_{c\text{-}Si}$) substrate remains unchanged, as is illustrate in the inset of Fig. 1(e). In the following thermal relaxation process, interfacial thermal transport from silicene to substrate is the only channel for the thermal

energy dissipations in silicene. Temperatures of the supported silicene, top three layers of Si, and total energies of silicene (E_t) are recorded each time step for post-processing. The outputs are averaged every 100 time steps to suppress data noise. In order to obtain smooth temperature evolutions during thermal relaxation, a temperature difference ΔT ($T_{silicene} - T_{c\text{-}Si}$) > 300 K is found necessary. Temperatures of silicene and top layers of *c*-Si in the 50 ps thermal relaxation process are shown in Fig. 1(e). Given the temperature and energy evolutions of the silicene system, R between silicene/Si can be calculated using the equation

$$\partial E_t / \partial t = \mathrm{A} \cdot (T_{silicene} - T_{c-Si}) / \mathrm{R}\,, \tag{2}$$

where E_t is the system energy of the supported silicene and A is surface area. An instant R can be calculated at each time step according to the local energy changing rate and corresponding temperature difference. We have tried this method and found it subject to the noise in the energy decay and the calculated interface thermal resistance has very large uncertainty. As the energy decay is driven by the temperature difference $\Delta T = T_{silicene} - T_{c\text{-}Si}$, the silicene energy changes against $\int \Delta T dt$ can be plotted and it is observed that the E_t profile has a linear relationship with $\int \Delta T dt$. Each segment can represent the interfacial thermal transport efficiency at certain temperature levels, and it can be concluded that the thermal transport is very steady during the transient process and the overall fitting method can be used. Therefore, it is speculated that the overall system temperature has much larger effects than the transient temperature on interfacial thermal transport. If R has little variation within the temperature range during thermal relaxation, a constant R value can be substituted into Eq. (2) to predict the E_t profile. Under such scenario, the interfacial thermal resistance can be calculated by best fitting of the E_t profile using least square method (LSM).

Take the silicene/*c*-Si hybrid system as an example, after the system reaches thermal equilibrium and fully relaxed at temperature 300 K, a thermal impulse $\dot{q}$ = 3.16×10^{-4} W is imposed to the supported silicene for 50 fs. In the following 50 ps thermal relaxation, the energy decay profile of silicene is recorded and fitted using the integral form of Eq. (2),

$$E_t = E_0 + (A/R)\cdot\int_0^t (T_{silicene} - T_{\mathrm{c-Si}})\,\mathrm{d}t\,, \tag{3}$$

where E_0 is the initial energy of the fitting process; $T_{silicene}$, $T_{c\text{-}Si}$ are illustrated in Fig 1. (e). The total energy (E_t) fitting results are shown in Fig. 2(a). It can be observed that the fitting curve soundly matches the calculated MD results, indicating the validity of Eq. (2) to describe this physical process. The averaged R results from five independent simulations equals 1.888 × 10^{-8} K·m^2/W with a standard deviation of 0.072, which is slightly lower than that between graphene/*c*-Si (3.52 × 10^{-8} K·m^2/W) at 300 K.[39] At the beginning stage of the fitting process, there is a small mismatch between the fitting curve and the calculated E_t results. This is due to the fact that after the 50 fs ultrafast heating process, kinetic and potential energies in silicene is in non-equilibrium state and the calculated MD temperatures are inaccurate. The observed fitting mismatch at early state will not affect the overall fitting result since it only lasts for several picoseconds. Energy fitting results for silicene on *a*-Si, *c*-SiO_2 and *a*-SiO_2 are shown in Figs. 2(b)-(d).

In practical applications, silicene-based devices are often placed in various working conditions at different temperatures. Thus it is of great interest to investigate temperature's effect on

interfacial thermal transport. The initial temperatures of the MD systems are adjusted to 100 K, 150 K, 200 K, 250 K, 350 K and 400 K for thermal contact resistance characterizations. To keep consistent with previous calculations, a 50 fs heat impulse with $\dot{q}$ = 3.16×10^{-4} W is used in all transient heating processes. Calculated R results are shown in Fig. 3. For each data point, five independent simulations are performed to gain the averaged results and standard deviations. It is concluded from the results that interfacial thermal resistance between silicene and Si/SiO_2 substrates decrease monotonically with temperature. Maximum R decreases of 28.7%, 28.4%, 36.9% and 31.4% are calculated for c-Si, a-Si, c-SiO_2 and a-SiO_2 substrates respectively. This temperature dependence of R is in good consistence of previous calculations between silicene/graphene, graphene/copper and carbon nanotube (CNT)/SiO_2.[41-43] To better explain temperature's effect on thermal resistance, phonon density of state (PDOS) of silicene supported on a-Si and a-SiO_2 at temperature 100 K and 400 K are analyzed. The PDOS can be calculated by taking the Fourier transform of the velocity autocorrelation function (VACF)

$$F(\omega) = 1/\sqrt{2\pi}\int_{-\infty}^{\infty} dt e^{i\omega t} Z(\mathrm{t}), \tag{4}$$

where $Z(\mathrm{t}) = < v(0)\cdot v(\mathrm{t}) > / < v(0)\cdot v(0) >$. Higher values of PDOS for a phonon with frequency ω means more states are occupied by it. And zero PDOS means there is no phonon with frequency ω exists in the system. The phonon power spectrum analysis provides a quantitative means to assessing the power carried by phonons in a system. It is observed in Fig. 4(a) that at temperature 100 K, the phonon PDOS of silicene and silicon are mainly distributed in the region of 0 – 20 THz, which is the same as reported by previous studies.[43-45] Since the phonon frequency does not depend on the amplitude of the oscillations, the PDOS of harmonic systems should be temperature-independent. However, when temperature increases to 400 K, it is

observed that both the PDOS of silicene and *a*-Si become broader, which indicates that the umklapp scattering mechanism is dominate at this temperature range and the phonon anharmonicity is significant. The umklapp processes reduces the phonon mean free paths (MFP) on both sides of the interface and altered the PDOS distribution with more activated higher frequency phonons. Contributions from the high frequency phonons to thermal transport reduce the thermal contact resistance. Moreover, the three phonon scatterings becomes more furious at high temperatures, which will decompose the high frequency phonons into lower frequency branches and couple with the other phonons in the hybrid system, and as a result decrease the value of *R*.

One of the crucial factors in determining the interfacial thermal resistance is the overlap of phonon states. To help compare the differences between the calculated results, the PDOS distributions are normalized with an integration area of 1 for each PDOS profile. If the phonon population of with certain ω value is low or zero, the energy propagation by phonons of that wave vector will be highly restricted. Therefore, the overlap areas between the PDOS with temperature need to be explored. To quantify this variation, an arbitrary unit variable, which is defined as $\delta = \int \omega A(\omega) d\omega$, is introduced to help assist the analyses.[46] $A(\omega)$ represents the intersection area at frequency ω. The area integration is proportional to the amount of energy transported across the interface by phonons at these frequency intervals. The calculated δ equals 0.81278 for silicene/*a*-Si at temperature 100 K and 0.86695 at temperature 400 K. Similar conclusions can be achieved from Fig. 4(c)-(d) for silicene/*a*-SiO_2. The PDOS overlap areas are calculated at 0.65979 and 0.68662 at temperatures 100 K and 400 K separately. The calculated

results are summarized in Table 1. It should be paid much attention that the size effect of silicene could be important in our silicene-substrate system and thus affect our calculation about the temperature dependence of interfacial thermal transport. To address this concern, different thickness values of 50 and 70 Å (for silicene) are applied in calculations and the results are shown in Fig. 3(c). It is found that no obvious variation for interfacial thermal resistance is observed. Therefore, it can be regarded that the calculated interfacial thermal resistance for the domain calculated in this work is not size-dependent.

Aside from the decreasing trend of R with temperature, another important discovery in this work is that the interfacial thermal resistances at amorphous interfaces are much lower than those at crystalline interfaces, as shown in Fig. 3. This phenomenon has also been reported in previous studies between graphene and SiC substrate.[46] This new discovery is contradictory to the traditional thought that amorphous structures always have worse thermal performance than crystalline structures. It is reported that the thermal conductivity of *a*-Si is only about one-hundredth of that of *c*-Si.[47] While when it comes to interfacial thermal transport at cross-plane direction, the amorphous structures can facilitate the thermal transport across interfaces. The disordered atomic structure greatly enhances the phonon scatterings in the amorphous system. The shortened phonon mean free path and phonon relaxation time will give rise to decreased in-plane thermal conductivities. Meanwhile, it decomposes the high frequency phonons into multiple low frequency branches and couples with other phonons, which directly contribute to interfacial thermal transport.

Similar to those peculiar thermal properties of graphene,[48-50] in a recent study by Hu *et al*.[51], a counter-intuitive phenomenon, in which the in-plane thermal conductivity (κ) of supported silicene can be either enhanced or suppressed by changing the surface crystal plane of the substrate, has been observed. By increasing the interfacial coupling strength (χ) in the 12-6 LJ potential, it is calculated that κ of silicene increases on 6H-SiC substrates and decreases on 3H-SiC substrates. This bilateral substrate effect is fundamentally different from that of previous graphene studies, which proved that substrates will always have negative effects on phonon transport in laterals directions.[52-54] In spite of this new discovery on the in-plane thermal transport of supported silicene, the coupling strength's effect on the out-of-plane thermal transport has not yet been studied. In this work, dependence of interfacial thermal resistance on coupling strength (χ) is calculated for *c*-Si, *a*-Si, *c*-SiO_2 and *a*-SiO_2 substrates. The initial temperature for all hybrid systems is set as 300 K. Different coupling strengths of χ = 1.0, 1.5 and 2.0 are applied. The calculated results are shown in Fig. 5. It is observed that the thermal contact resistance decreases monotonically with χ, indicating no bilateral effects for the substrates used in this work. The maximum decrease of *R* is calculated at 35.9%, 43.5%, 29.4% and 38.1% for silicene/*c*-Si, silicene/*a*-Si, silicene/*c*-SiO_2 and silicene/*a*-SiO_2 respectively. The stronger coupling strength enhanced the phonon couplings at the interface, which directly contributes to the interfacial thermal transport and reduces the calculated *R* results.

In this work, interfacial thermal transport across silicene and various crystalline and amorphous substrates are studied using classical MD simulations. A fast transient technique is applied to calculate the interfacial thermal resistance. Compared to traditional NEMD method, this

technique can characterize the resistance within only 50 ps with higher accuracy. Effects of temperature, substrate crystallinity, and coupling strength on cross-plane thermal transport are discussed. It is found out that interfacial thermal resistance decreases monotonically with temperature. And contradictory to the traditional thought amorphous structures always have negative effects on phonon thermal transport, it is calculated that amorphous silicon and silica can facilitate the interfacial thermal transport compared to their crystalline structures. The greater phonon scattering is the major factor that contributes to this peculiar phenomenon. Unlike the bilateral substrates effects reported on the in-plane thermal transport of silicene, the interfacial thermal resistances across silicene and *c*-Si, *a*-Si, *c*-SiO_2 and *a*-SiO_2 substrates have the same decreasing trend with enlarged coupling strength, which is the same as reported in previous studies of graphene structures.

ACKNOWLEDGEMENTS

J. Z. thanks the support from UNL Holland Computing Center. Z. X acknowledges the support from the National Natural Science Foundation of China (No. 51379160). H. B acknowledges the support from the National Natural Science Foundation of China (No. 51306111) and Shanghai Municipal Natural Science Foundation (No. 13ZR1456000). Y. Y thanks the support from the National Natural Science Foundation of China (Nos. 51206124 and 51428603). Y. Y appreciates the discussion with Prof. Nuo Yang from Huazhong University of Science and Technology.

References

[1] K. Takeda and K. Shiraishi, Physical Review B **50,** 14916 (1994).

[2] M. Hu, X. Zhang, and D. Poulikakos, Physical Review B **87,** 195417 (2013).

[3] A. Kara, H. Enriquez, A. P. Seitsonen, L. C. Lew Yan Voon, S. Vizzini, B. Aufray, and H. Oughaddou, Surface Science Reports **67,** 1 (2012).

[4] B. Lalmi, H. Oughaddou, H. Enriquez, A. Kara, S. Vizzini, B. Ealet, and B. Aufray, Applied Physics Letters **97,** 223109 (2010).

[5] H. P. Li and R. Q. Zhang, Epl **99,** 36001 (2012).

[6] T. Ng, J. Yeo, and Z. Liu, International Journal of Mechanics and Materials in Design **9,** 105 (2013).

[7] Q.-X. Pei, Y.-W. Zhang, Z.-D. Sha, and V. B. Shenoy, Journal of Applied Physics **114,** 033526 (2013).

[8] B. Liu, C. D. Reddy, J. W. Jiang, H. W. Zhu, J. A. Baimova, S. V. Dmitriev, and K. Zhou, Journal of Physics D-Applied Physics **47,** 165301 (2014).

[9] X. Gu and R. Yang, Journal of Applied Physics **117,** 025102 (2015).

[10] H. Xie, M. Hu, and H. Bao, Applied Physics Letters **104,** 131906 (2014).

[11] X. Zhang, H. Xie, M. Hu, H. Bao, S. Yue, G. Qin, and G. Su, Physical Review B **89,** 054310 (2014).

[12] J. Tersoff, Physical Review B **37,** 6991 (1988).

[13] Z. Wang, T. Feng, and X. Ruan, Journal of Applied Physics **117,** 084317 (2015).

[14] L. Hai-peng and Z. Rui-qin, EPL (Europhysics Letters) **99,** 36001 (2012).

[15] S. Cahangirov, M. Topsakal, E. Aktürk, H. Şahin, and S. Ciraci, Physical Review Letters **102,** 236804 (2009).

[16] J. C. Garcia, D. B. de Lima, L. V. C. Assali, and J. F. Justo, The Journal of Physical Chemistry C **115,** 13242 (2011).

[17] D. Kaltsas, L. Tsetseris, and A. Dimoulas, Applied Surface Science **291,** 93 (2014).

[18] T. Kumagai, S. Izumi, S. Hara, and S. Sakai, Computational Materials Science **39,** 457 (2007).

[19] M. I. Baskes, Physical Review B **46,** 2727 (1992).

[20] L. Bo, C. D. Reddy, J. Jinwu, Z. Hongwei, A. B. Julia, V. D. Sergey, and Z. Kun, Journal of Physics D: Applied Physics **47,** 165301 (2014).

[21] F. H. Stillinger and T. A. Weber, Physical Review B **31,** 5262 (1985).

[22] S. Plimpton, Journal of Computational Physics **117,** 1 (1995).

[23] S. Munetoh, T. Motooka, K. Moriguchi, and A. Shintani, Computational Materials Science **39,** 334 (2007).

[24] A. K. Rappe, C. J. Casewit, K. S. Colwell, W. A. Goddard, and W. M. Skiff, Journal of the American Chemical Society **114,** 10024 (1992).

[25] C. L. Lin, R. Arafune, K. Kawahara, N. Tsukahara, E. Minamitani, Y. Kim, N. Takagi, and M. Kawai, Applied Physics Express **5,** 045802 (2012).

[26] P. Vogt, P. De Padova, C. Quaresima, J. Avila, E. Frantzeskakis, M. C. Asensio, A. Resta, B. Ealet, and G. Le Lay, Physical Review Letters **108,** 155501 (2012).

[27] Q. Wang, C. Wang, Y. Zhang, and T. Li, Nuclear Instruments and Methods in Physics Research Section B: Beam Interactions with Materials and Atoms **328,** 42 (2014).

[28] S. S. Mahajan, G. Subbarayan, and B. G. Sammakia, Intersoc C Thermal T**,** 1055 (2008).

[29] J. C. Zhang and X. W. Wang, Nanoscale **5,** 734 (2013).

[30] B. Liu, J. A. Baimova, C. D. Reddy, S. V. Dmitriev, W. K. Law, X. Q. Feng, and K. Zhou, Carbon **79,** 236 (2014).

[31] Q. Y. Wang, C. L. Wang, Y. Zhang, and T. S. Li, Nuclear Instruments & Methods in Physics Research Section B-Beam Interactions with Materials and Atoms **328,** 42 (2014).

[32] Y. Ni, Y. Chalopin, and S. Volz, 6th European Thermal Sciences Conference (Eurotherm 2012) **395** (2012).

[33] S. Merabia and K. Termentzidis, Physical Review B **86,** 094303 (2012).

[34] S. S. Mahajan, G. Subbarayan, and B. G. Sammakia, 2008 11th Ieee Intersociety Conference on Thermal and Thermomechanical Phenomena in Electronic Systems, Vols 1-3**,** 1055 (2008).

[35] V. Samvedi and V. Tomar, Nanotechnology **20,** 365701 (2009).

[36] B. Liu, J. A. Baimova, C. D. Reddy, A. W. K. Law, S. V. Dmitriev, H. Wu, and K. Zhou, Acs Applied Materials & Interfaces **6,** 18180 (2014).

[37] J. Zhang, Y. Hong, and Y. Yue, Journal of Applied Physics **117,** 134307 (2015).

[38] B. Liu, F. Meng, C. D. Reddy, J. A. Baimova, N. Srikanth, S. V. Dmitriev, and K. Zhou, RSC Advances **5,** 29193 (2015).

[39] J. Zhang, Y. Wang, and X. Wang, Nanoscale **5,** 11598 (2013).

[40] Y. Hong, L. Li, X. C. Zeng, and J. Zhang, Nanoscale **7,** 6286 (2015).

[41] L. Chen, Z. Huang, and S. Kumar, Applied Physics Letters **103,** 123110 (2013).

[42] Z.-Y. Ong and E. Pop, Physical Review B **81,** 155408 (2010).

[43] B. Liu, J. A. Baimova, C. D. Reddy, A. W.-K. Law, S. V. Dmitriev, H. Wu, and K. Zhou, ACS Applied Materials & Interfaces **6,** 18180 (2014).

[44] H. P. Li and R. Q. Zhang, Epl **105,** 56003 (2014).

[45] Y. Zhang, J. X. Cao, Y. Xiao, and X. H. Yan, Journal of Applied Physics **102,** 104303 (2007).

[46] M. Li, J. Zhang, X. Hu, and Y. Yue, Applied Physics A **119,** 415 (2015).

[47] H. Wada and T. Kamijoh, Japanese Journal of Applied Physics Part 2-Letters **35,** L648 (1996).

[48] Y. Yue, J. Zhang, X. Tang, S. Xu, and X. Wang, Nanotechnology Reviews**,** DOI: 10.1515/ntrev (2015).

[49] J. Zhang, X. Wang, and H. Xie, Physics Letters A **377,** 721 (2013).

[50] J. Zhang, X. Wang, and H. Xie, Physics Letters A **377,** 2970 (2013).

[51] X. Zhang, H. Bao, and M. Hu, Nanoscale **7,** 6014 (2015).

[52] K.-X. Chen, X.-M. Wang, D.-C. Mo, and S.-S. Lyu, Chemical Physics Letters **618,** 231 (2015).

[53] Z.-X. Guo, J. W. Ding, and X.-G. Gong, Physical Review B **85,** 235429 (2012).

[54] E. Pop, V. Varshney, and A. K. Roy, Mrs Bulletin **37,** 1273 (2012).

List of Table and Figures

SiO_2 at temperatures 100 K and 400 K. It can be observed that as temperature increases, the PDOS of both silicene and substrates are broadened. Meanwhile, the overlap area δ becomes larger with temperature, indicating better phonon transmissions across the interfaces. The calculated δ values are displayed in Table 1.

Figure 5 Interfacial thermal resistance variations with LJ coupling strength χ.

$\delta = \int \omega A(\omega) d\omega$	100 K	400 K
a-Si	0.81278	0.86695
a-SiO_2	0.65979	0.68662

Table 1. Comparison of the transmitted phonon energy through the interface: the integration of the overlap area multiplied by the corresponding frequency in PDOS of the interface materials

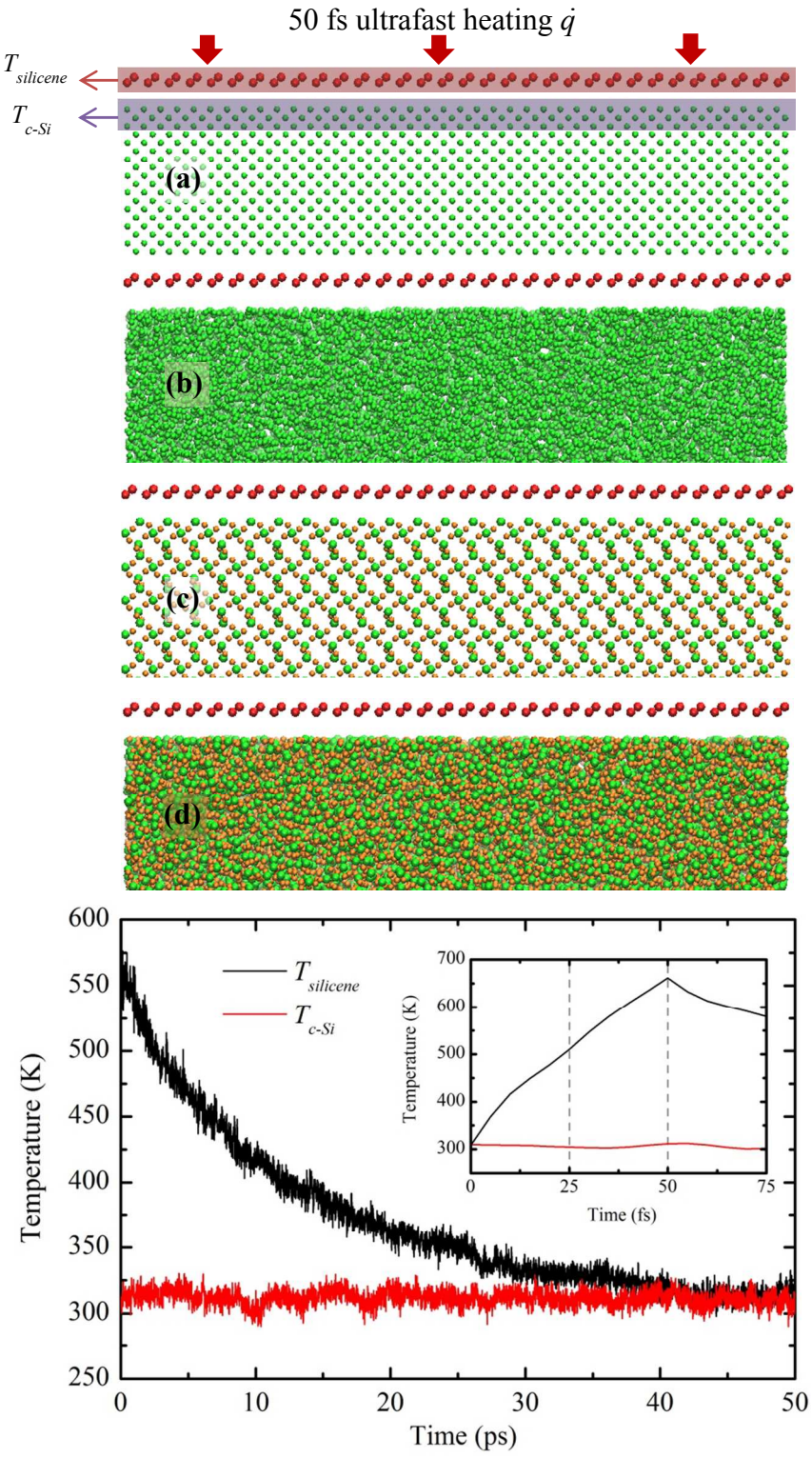

Figure 1. (a)-(d) Atomic configurations of silicene/*c*-Si, silicene/*a*-Si, silicene/*c*-SiO_2 and silicene/*a*-SiO_2 hybrid systems. Periodic boundaries are applied to the lateral (*x* and *y*) directions. Free boundary condition is used in the out-of-plane (*z*) direction. (e) Illustration of the transient heating technique for the silicene/*c*-Si system.

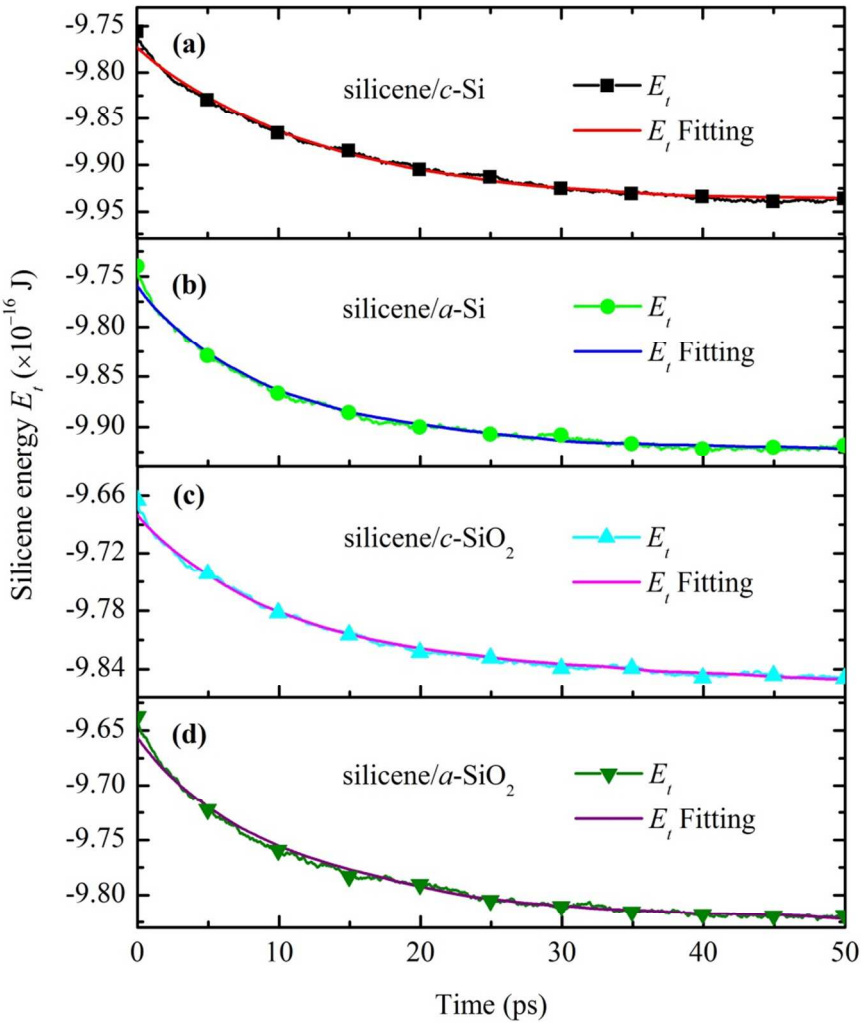

Figure 2. (a)-(d) Energy fitting results of supported silicene for different hybrid systems at temperature 300 K. MD energy outputs are represented by dot-line profiles. Solid lines represent the fitting curves.

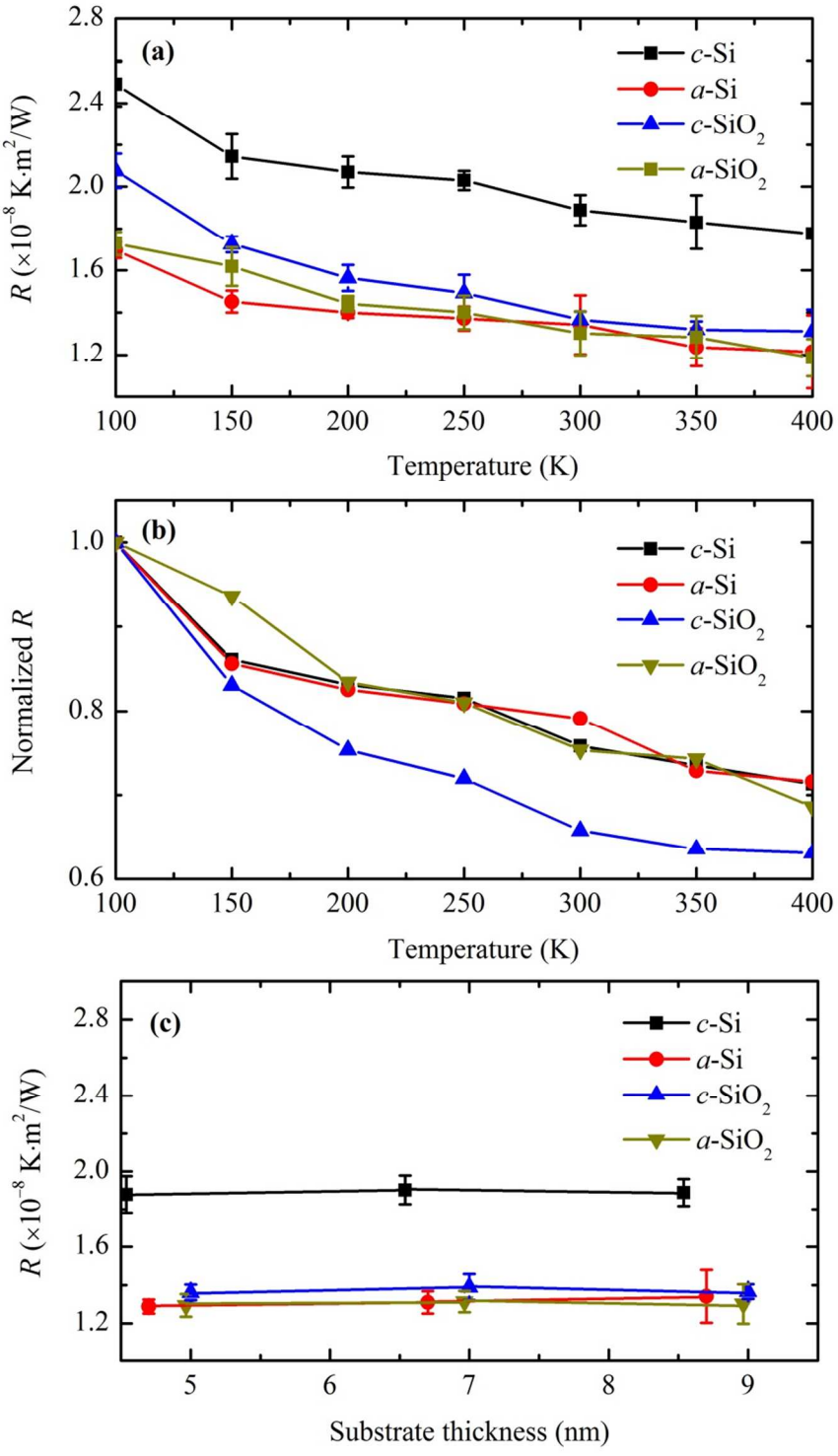

Figure 3. (a) Dependence of interfacial thermal resistance (R) with temperature. Five independent simulations are performed on each case. The averaged results and standard

deviations are represented by solid dots and error bars respectively. (b) Normalized *R* values with temperature. It can be observed that the *c*-Si, *a*-Si and *a*-SiO_2 substrates have similar effects on interfacial thermal resistance from 100 K to 400 K, while the silicene/*c*-SiO_2 heterostructure has a faster *R* drop within the same temperature range. (c) Substrate thickness effects on *R*. When thickness decreases to ~5 nm and ~7 nm, the calculated *R* results do not have substantial changes, indicating size-independent *R* values in the out-of-plane *z* direction.

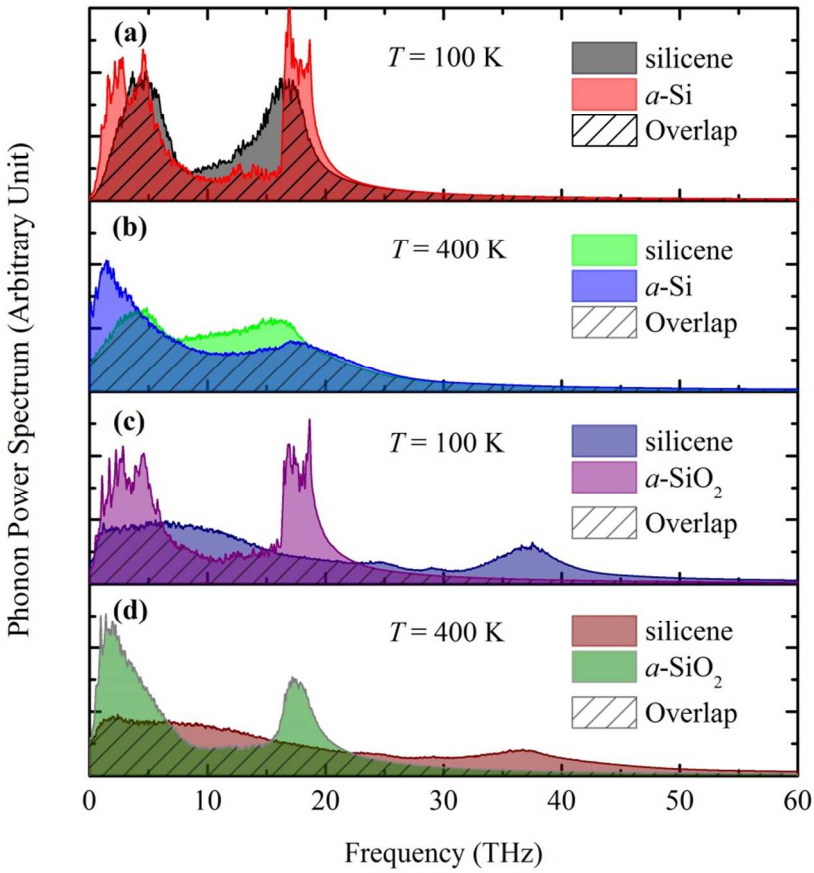

Figure 4. (a), (b) Phonon power spectra for silicene and top layers of *a*-Si at temperatures 100 K and 400 K. (c), (d) Phonon power spectra for silicene and top layers of *a*-SiO_2 at temperatures 100 K and 400 K. It can be observed that as temperature increases, the PDOS of both silicene and substrates are broadened. Meanwhile, the overlap area δ becomes larger with temperature, indicating better phonon transmissions across the interfaces. The calculated δ values are displayed in Table 1.

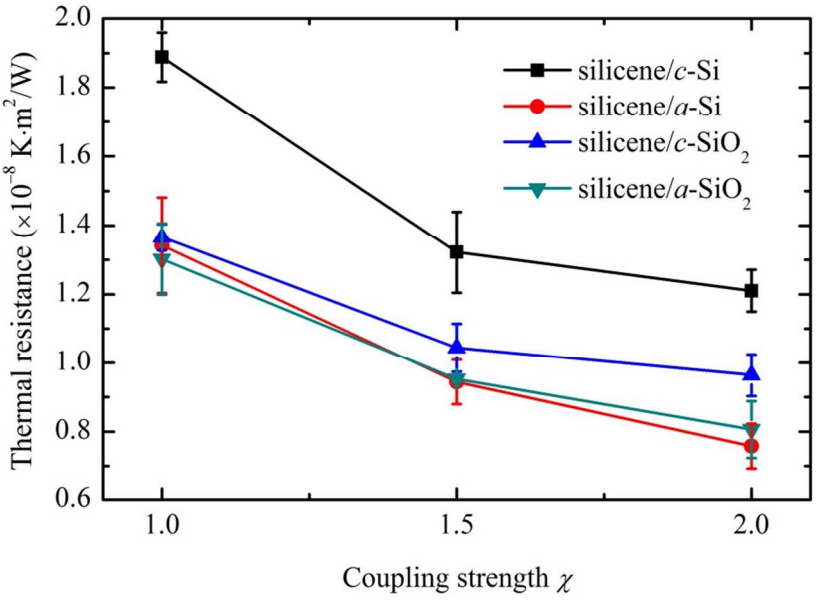

Figure 5. Interfacial thermal resistance variations with LJ coupling strength χ.